Phys. Scr. **77** (2008) 055302 (10pp) doi:10.1088/0031-8949/77/05/055302

Spectrum and energy levels of the Nd^{4+} free ion (Nd V)

Ali Meftah[1], **Jean-François Wyart**[1], **Jocelyne Sinzelle**[1], **Wan-Ü Lydia Tchang-Brillet**[2], **Norbert Champion**[2], **Nissan Spector**[3] and **Jack Sugar**[3]

[1] Laboratoire Aimé Cotton, CNRS, Bâtiment 505, Univ Paris-Sud, 91405 Orsay Cedex, France
[2] LERMA, UMR8112 du CNRS, Observatoire de Paris-Meudon, Université Pierre et Marie Curie-Paris 6, F-92195 Meudon, France
[3] National Institute of Standards and Technology, Gaithersburg, MD 20899-8422, USA

E-mail: ali.meftah@lac.u-psud.fr

Received 9 October 2007
Accepted for publication 18 March 2008
Published 29 April 2008
Online at stacks.iop.org/PhysScr/77/055302

Abstract
The spectrum of neodymium excited by a sliding spark source was photographed on two vacuum ultraviolet normal-incidence spectrographs. About 250 lines attributed to Nd V, hitherto unknown, have been identified. The analysis of this spectrum established all the energy levels of the configurations $4f^2$, 4f5d, 4f6s and 4f6p (except for $4f^2\ ^1S_0$). Altogether, 48 known levels classify about 160 lines. Their theoretical calculation includes a least-squares fit with an rms error of 28 cm^{-1} for the even-parity levels and 26 cm^{-1} for the odd-parity ones, as well as the best values for relevant radial interaction parameters. In particular, interactions with the core-excited configurations $5p^54f^3$ and $5p^54f^25d$ are discussed. Intensities derived from phosphor image plates are used to estimate an effective temperature in the spark of $T_{\mathrm{eff}} = 3.6$ eV.

PACS numbers: 31.15.Md, 32.30.Jc, 32.70.Cs, 42.55.Rz, 52.80.Yr

1. Introduction

Except for La V, Ce V, Pr V and Lu V, all the spectra of the four-times ionized lanthanides are still unknown. Among the known spectra, La V and Ce V have $5p^5$ and $5p^6$ ground configurations, respectively, and only Pr V and Lu V have a ground configuration of the type $4f^N$, with a doublet $4f\ ^2F$ for Pr V and a doublet $4f^{13}\ ^2F$ for Lu V. The present work on neodymium describes, for the first time, the fifth spectrum of a lanthanide element with more than two levels in its ground configuration. In the recent analysis of Nd IV [1, 2], the presence of a transition array in the wavelength region 700–1000 Å appearing at higher excitation than Nd^{3+} was mentioned. Its attribution to Nd V is now confirmed.

2. Experiment

The spectrum of neodymium had been first recorded in the wavelength region 500–2700 Å on the 10.7 m normal incidence spectrograph with photographic plates (PPs) at the National Bureau of Standards (NBS) some years ago, with the aim of extending the sequence of two-electron spectra La II, Ce III and Pr IV [3] to Nd V. This instrument was equipped with a 1200 lines mm^{-1} ruled concave grating and provided a plate factor of 0.78 Å mm^{-1} in the first order. The ionized neodymium spectrum in emission was obtained using a vacuum sliding spark source [4, 5]. The source operating conditions were varied to produce peak currents of 50, 200, 500 and 1200 A in order to favour different ionization stages. More recently, new spectra were recorded at the Paris-Meudon Observatory with a similar light source. The vacuum spectrograph in these experiments differed from the NBS instrument by a 3600 lines mm^{-1} holographic concave grating, leading to a linear dispersion of 0.26 Å mm^{-1} on the plates. For some exposures, phosphor-storage image plates (IP) were used for intensity measurements [6]. Wavelength measurements of the photographic spectra were made on a semi-automatic photoelectric comparator. The spectra were calibrated by polynomial interpolation of reference line wavelengths [7] from ionized low-Z elements (C, N, O, Al, Si) present in the Nd tracks. The typical uncertainty on measured wavelengths for isolated lines of average intensities can be estimated from the standard deviation of the quadratic fit of the reference wavelengths.

It is about 0.004 Å in the 700–1000 Å region, limited by the quality of oxygen and nitrogen wavelengths used as references, and deteriorates to about 0.008 Å around 2000 Å because of the scarcity of references. In the short-wavelength region of the neodymium spectrum, a dense transition array at 700–750 Å appears on the plates with comparable intensities in the two tracks with peak current of 1200 and 500 A. It is presumably due to the $4f^2 5f$–$4f^2 5d$ transitions in Nd IV that have not yet been analysed. At slightly longer wavelengths, several tens of lines appear only in the 1200 A track. Their wavelength range agreed with that of the theoretical predictions for both the $4f^2$–4f5d and 4f5d–4f6p transitions of Nd V. Around 1900 and 2200 Å, the 4f6s–4f6p transitions are present in the 1200 A track only.

3. Determination of energy levels and classification of spectral lines

Cowan's method and codes [8] were used to determine the lowest configurations and spectral ranges of their transitions in Nd V. In order to be consistent with what was done in the Nd IV case [1, 2], the Hartree–Fock code RCN was run in the HFR relativistic mode without including Breit energies and setting the correlation term to a value of 1.0. This step of calculations led to average energies and radial parameters for the two-electron configurations $4f^2$, 4f5d, 4f6s, 4f6p and $(5d+6s)^2$, which continue the known isoelectronic sequence of La II. The trends to hydrogenic reordering of orbital energies with increasing ionic charge results in a 5p–4f excitation energy smaller in Nd V than in the lower ionization stages, and also in lower energies predicted for configurations of both the parities with open subshell $5p^5$. Following this first step, a straight diagonalization of the Hamiltonian, by means of Cowan's RCG code and using the HFR radial integrals as input data, places all the levels of $5p^5 4f^3$ (97000–237000 cm^{-1}) at lower energies than those of $5p^6 4f6p$ (239000–251000 cm^{-1}). In order to obtain improved-level predictions, as input data for the RCG code, the HFR radial parameter values for Nd V were scaled by factors derived from general trends established in Pr IV [9], Nd IV [1, 2], Yb IV [10], Ce V [11] and in other known lanthanide spectra. The well-predicted wavelengths and intensities led us to the identification of the $4f^2\,{}^3H$–$4f5d\,{}^3G$ transitions and to the determination of fine structure intervals of these terms. Starting from these first-known levels, the application of the Ritz combination principle led to the determination of other levels from the $4f^2$–4f5d and 4f5d–4f6p transition arrays. The 4f6s levels were established in the last stage of the analysis.

In the present work, 48 new levels, i.e. 12 out of the 13 levels of the ground configuration $4f^2$ as well as all the 36 levels of the configurations 4f5d, 4f6p and 4f6s have been established. Only the highest level of the ground configuration $4f^2\,{}^1S_0$ remains unknown, since it should be established by a single $4f^2\,{}^1S_0 - 4f5d\,{}^1P_1$ transition, which could not be firmly identified.

The optimized values for the 48 levels were calculated with the ELCALC code[4] which applies an iterative procedure to minimize the differences between observed wavenumbers and those calculated from level energies. As an input to the ELCALC code, together with the initial approximate E_{exp} level values, the wavenumbers of 140 isolated lines were given with uncertainties smoothly decreasing from 0.60 to 0.20 cm^{-1} between 720 and 2300 Å, according to the estimates given in section 2. The results of the ELCALC code were optimized level values and for each level, the uncertainty derived from the standard deviation of the wavenumbers involved for its calculation. They are listed in table 1 for the even parity and in table 2 for the odd parity. The optimization procedure and the derivation of level value uncertainties are described by Radziemski and Kaufman [12]. The customary unit cm^{-1} for level energies used here is related to the unit for energy (joule) by $1\,cm^{-1} = 1.986445501(99) \times 10^{-23}$ J [13].

Table 3 contains 157 observed lines that were classified by the 48 new levels in Nd V, six of these lines having double classifications. We give their transition wavelengths and their relative intensities derived from visual estimates of photographic plate (PP) blackening, in the same way as in Kelly's table [7], over a scale of 1–1000 and from IPs when available. In the absence of calibration and of correction for plate sensitivity versus wavelength, the visual estimates Int_{PP} are consistent within limited wavelength range and should be assigned an uncertainty of about 30%. As concerns the IP, which has a linear intensity response [6], the Int_{IP} values have a noise level of about 5 in our arbitrary units. The comments after the wavelengths explain several deviations between wavelengths calculated from the levels and the measured ones. They are: p, line resolved on the plate, but perturbed by a close line; bl, line partially resolved in a blended emission peak with components of similar intensities; a, an asymmetric line, meaning that the components of the blend have different intensities.

4. Theoretical interpretation of the energy levels

The theoretical interpretation of energy levels in Nd V was carried out with an iterative least-squares fitting of the theoretical level values to the experimental ones by treating the radial integrals as adjustable parameters, a method used first by Racah in another two-electron spectrum Th III [14]. This parametric study proceeded by means of Cowan's codes RCG and RCE. We used two different bases of configurations. The first one was simply a two-configuration basis, i.e. $(4f^2 + 4f6p)$ in even parity and $(4f5d + 4f6s)$ in odd parity. In the second one we added six configurations in even parity: the first three ($5p^6 5d^2$, $5p^6 5d6s$ and $5p^6 6s^2$) are low configurations in La II and Ce III, where they mix with $5p^6 4f^2$ and $5p^6 4f6p$. Although they are unknown in Pr IV, it seemed interesting for isoelectronic comparisons to have them present in the study of Nd V. The last even configurations added were the core-excited ones $5p^5 4f^3$, $5p^5 4f^2 6p$ and $5p^5 4f5d^2$. This led to matrices of 208×208 maximum size and more than 120 radial parameters, which could be handled by Cowan's diagonalization code RCG.

In the odd parity (see table 2), the lowest configurations with an open 5p subshell, i.e. $5p^5 4f^2 5d$ and $5p^5 4f^2 6s$ were added to $5p^6 4f5d$ and $5p^6 4f6s$. The number of parameters increased considerably and all of them were fixed at scaled

[4] The procedure and definition of the level values uncertainties are described by Radziemski and Kaufman [12].

Table 1. Even-parity energy levels of the two configurations $4f^2$ and 4f6p of Nd^{4+}. For each level is given energy value and corresponding uncertainties in parenthesis (in cm^{-1}), N, the number of transitions involved in its calculation and g_{calc}, the calculated Landé factor. The deviations (in cm^{-1}) $\Delta E = E_{exp} - E_{calc}$ use E_{calc} values derived by means of the Cowan codes [8] with parameters given in table 4. The leading components of the eigenfunctions are given in the LS coupling scheme. The percentages of squared components in the four configurations $4f^2$, 4f6p, $5p^54f^3$ and $5p^54f^26p$ are given in the last columns.

								Percentage composition			
Conf.	J	E_{exp} (unc.)	N	g_{calc}	ΔE	1st comp.	%	$4f^2$	4f6p	p^5f^3	p^5f^2p
$4f^2$	4	0.00(26)	8	0.806	−33	$(^1S)^3H$	96.4	99.56	0.00	0.14	0.11
$4f^2$	5	2834.29(31)	6	1.033	9	$(^1S)^3H$	99.6	99.57	0.00	0.14	0.11
$4f^2$	6	5743.41(39)	3	1.166	27	$(^1S)^3H$	99.2	99.57	0.00	0.14	0.11
$4f^2$	2	5893.82(29)	5	0.675	3	$(^1S)^3F$	96.8	99.45	0.00	0.24	0.11
$4f^2$	3	7784.82(28)	9	1.084	16	$(^1S)^3F$	99.5	99.46	0.00	0.24	0.11
$4f^2$	4	8311.43(26)	9	1.156	−48	$(^1S)^3F$	63.6	99.50	0.00	0.19	0.11
$4f^2$	4	12269.73(26)	7	1.088	26	$(^1S)^1G$	62.4	99.55	0.00	0.15	0.11
$4f^2$	2	20551.37(25)	8	1.040	8	$(^1S)^1D$	87.1	99.19	0.00	0.49	0.11
$4f^2$	0	25050.63(41)	3	–	61	$(^1S)^3P$	97.7	98.97	0.00	0.68	0.13
$4f^2$	1	25892.92(34)	5	1.501	12	$(^1S)^3P$	99.0	98.99	0.00	0.66	0.13
$4f^2$	6	26088.12(48)	2	1.001	−2	$(^1S)^1I$	99.0	99.31	0.00	0.39	0.11
$4f^2$	2	27478.68(25)	6	1.452	−80	$(^1S)^3P$	89.4	99.02	0.00	0.63	0.13
4f6p	3	238688.04(13)	6	0.849	−18	$(^2F)^3G$	64.0	0.00	99.24	0.15	0.50
4f6p	2	239232.46(13)	6	0.811	11	$(^2F)^3F$	63.6	0.00	99.25	0.20	0.40
4f6p	3	242694.90(13)	13	1.156	−9	$(^2F)^3F$	45.7	0.00	99.22	0.21	0.44
4f6p	4	243086.98(18)	10	1.113	16	$(^2F)^3G$	46.7	0.00	99.24	0.21	0.44
4f6p	3	245187.54(13)	5	0.958	−16	$(^2F)^3F$	33.8	0.00	99.35	0.11	0.42
4f6p	2	246362.22(21)	9	0.976	38	$(^2F)^3D$	50.1	0.00	99.11	0.12	0.61
4f6p	4	246677.55(15)	10	1.076	0	$(^2F)^3G$	51.2	0.00	99.21	0.14	0.53
4f6p	1	247130.74(19)	6	0.499	−15	$(^2F)^3D$	98.9	0.00	98.92	0.12	0.79
4f6p	3	249730.10(14)	6	1.204	−6	$(^2F)^3D$	58.8	0.00	99.14	0.12	0.59
4f6p	4	249919.57(13)	8	1.112	−6	$(^2F)^1G$	54.9	0.00	99.27	0.20	0.41
4f6p	5	250015.66(20)	6	1.200	18	$(^2F)^3G$	99.2	0.00	99.21	0.07	0.60
4f6p	2	251562.98(27)	7	1.046	−13	$(^2F)^1D$	62.1	0.00	99.03	0.09	0.68

Table 2. Odd-parity energy levels of the two configurations 4f5d and 4f6s of Nd^{4+}. For each level is given energy value and corresponding uncertainties in parenthesis (in cm^{-1}), N, the number of transitions involved in its calculation and g_{calc}, the calculated Landé factor. The deviations (in cm^{-1}) $\Delta E = E_{exp} - E_{calc}$ use E_{calc} values derived by means of the Cowan codes [8] with parameters given in table 4. The leading components of the eigenfunctions are given in the LS coupling scheme. The percentages of squared components in the four configurations 4f5d, 4f6s, $5p^54f^25d$ and $5p^54f^26s$ are given in the last column.

								Percentage composition			
Conf.	J	E_{exp} (unc.)	N	g_{calc}	ΔE	1st comp.	%	4f5d	4f6s	p^5f^2d	p^5f^2s
4f5d	2	127558.79(33)	7	0.769	−3	$(^2F)^3F$	65.5	98.47	0.00	1.52	0.01
4f5d	4	127565.05(23)	7	0.921	−25	$(^2F)^1G$	55.4	98.60	0.00	1.39	0.01
4f5d	3	129104.48(25)	7	0.785	16	$(^2F)^3G$	85.1	98.13	0.00	1.86	0.01
4f5d	4	130552.98(24)	9	0.926	10	$(^2F)^3H$	58.7	98.43	0.00	1.56	0.01
4f5d	3	131104.67(33)	9	1.067	−2	$(^2F)^3F$	92.5	98.60	0.00	1.40	0.01
4f5d	4	132162.06(26)	10	1.058	−4	$(^2F)^3G$	93.1	98.04	0.00	1.95	0.01
4f5d	2	132565.78(32)	7	0.949	16	$(^2F)^1D$	53.7	98.01	0.00	1.98	0.01
4f5d	5	132597.49(33)	5	1.034	2	$(^2F)^3H$	97.5	98.25	0.00	1.74	0.01
4f5d	1	133366.26(28)	6	0.545	20	$(^2F)^3D$	90.3	97.65	0.00	2.34	0.01
4f5d	4	134359.66(21)	11	1.195	15	$(^2F)^3F$	77.8	98.60	0.00	1.39	0.01
4f5d	5	135027.22(26)	9	1.193	−11	$(^2F)^3G$	94.0	97.95	0.00	2.04	0.01
4f5d	3	135318.28(19)	11	1.205	25	$(^2F)^3D$	63.5	97.90	0.00	2.08	0.01
4f5d	2	135359.21(26)	7	1.161	−36	$(^2F)^3D$	86.0	97.67	0.00	2.32	0.01
4f5d	6	136363.39(36)	3	1.167	−2	$(^2F)^3H$	98.2	98.22	0.00	1.78	0.01
4f5d	1	138275.39(29)	6	1.429	1	$(^2F)^3P$	87.4	97.35	0.00	2.64	0.01
4f5d	0	138519.19(67)	2	–	−14	$(^2F)^3P$	97.3	97.32	0.00	2.67	0.01
4f5d	3	139549.81(31)	9	1.110	−16	$(^2F)^1F$	61.1	98.07	0.01	1.91	0.01
4f5d	2	140180.78(40)	6	1.455	16	$(^2F)^3P$	88.6	97.39	0.00	2.61	0.01
4f5d	5	142910.77(33)	8	1.007	0	$(^2F)^1H$	94.4	97.72	0.00	2.28	0.00
4f5d	1	147601.42(31)	4	1.026	−1	$(^2F)^1P$	87.5	98.06	0.00	1.93	0.01
4f6s	2	193598.54(10)	5	0.764	−26	$(^2F)^3F$	86.7	0.00	86.66	13.09	0.24
4f6s	3	194029.49(11)	4	1.110	34	$(^2F)^3F$	42.8	0.02	61.35	38.46	0.16
4f6s	4	197452.83(11)	6	1.217	17	$(^2F)^3F$	61.7	0.03	61.74	38.09	0.15
4f6s	3	197997.88(13)	5	1.012	−11	$(^2F)^1F$	56.4	0.03	78.90	20.85	0.22

Table 3. Classified lines of Nd V. The experimentally measured wavelengths (λ_{exp} in Å) are in air above 2000 Å. They are followed by the deviations $\Delta\lambda = \lambda_{exp} - \lambda_{Ritz}$ from the Ritz wavelengths (in mÅ), intensities in arbitrary units (PP : photographic plate; IP : image plate; see text), calculated transition probabilities gA (in 10^6 s^{-1}), g being the statistical weight of the upper level. The CI columns include the interactions within 12 configurations, whereas the no–CI values do not. The experimental wavenumbers σ_{exp} and the combining odd-level and even-level energies (E^o and E^e, respectively) are in cm^{-1}. The level identifications are detailed in tables 1 and 2. The comments after the wavelengths are explained at the end of the table.

λ_{exp} (Å)	$\Delta\lambda$ (mÅ)	Int_{exp} PP	IP	Int cal	gA_{CI}	gA_{no-CI}	σ_{exp} (cm^{-1})	E^o (cm^{-1})	J	E^e (cm^{-1})	J
713.891	−5	2		1	5	12	140077.4	142910.77	5	2834.29	5
729.036 p	0	20		9	62	258	137167.4	142910.77	5	5743.41	6
738.999	0	2		6	32	113	135318.2	135318.28	3	0.00	4
742.942	−3	2		5	32	35	134600.0	142910.77	5	8311.43	4
744.269	−2	1		4	20	72	134360.0	134359.66	4	0.00	4
748.900	0	30		6	30	120	133529.1	136363.39	6	2834.29	5
754.159	−3	8		6	30	115	132598.0	132597.49	5	0.00	4
756.472	2	25		19	98	340	132192.6	135027.22	5	2834.29	5
756.650	3	30		20	91	316	132161.5	132162.06	4	0.00	4
758.925	−2	3		4	24	70	131765.3	139549.81	3	7784.82	3
760.311	2	50		29	142	476	131525.1	134359.66	4	2834.29	5
761.971	−1	3		3	18	59	131238.6	139549.81	3	8311.43	4
762.753	4	60		35	153	534	131104.1	131104.67	3	0.00	4
765.456	0	40		28	186	291	130641.1	142910.77	5	12269.73	4
765.579	−1	100		177	935	3913	130620.1	136363.39	6	5743.41	6
765.973	1	40		56	239	1077	130552.8	130552.98	4	0.00	4
770.635	0	100		171	788	3336	129763.2	132597.49	5	2834.29	5
773.230	1	200		714	3230	12370	129327.6	132162.06	4	2834.29	5
773.493	1	250		818	4084	15580	129283.7	135027.22	5	5743.41	6
774.567	0	200		617	2505	9544	129104.4	129104.48	3	0.00	4
783.863 p	6	50		183	913	3266	127573.4	135359.21	2	7784.82	3
783.912 p	−2	40		108	413	1724	127565.4	127565.05	4	0.00	4
784.105	−3	12		16	81	302	127533.9	135318.28	3	7784.82	3
784.483	0	80		150	697	2495	127472.4	133366.26	1	5893.82	2
785.669	0	150		353	2025	7159	127280.1	139549.81	3	12269.73	4
787.091	−1	60		62	466	1255	127050.1	147601.42	1	20551.37	2
787.359	0	150		352	1741	6256	127006.9	135318.28	3	8311.43	4
789.169	2	50		53	260	625	126715.5	135027.22	5	8311.43	4
789.440	−1	20		15	68	317	126672.0	132565.78	2	5893.82	2
790.043	−4	8		7	32	160	126575.4	134359.66	4	7784.82	3
793.348	1	60		83	394	1500	126048.1	134359.66	4	8311.43	4
798.654	1	15		9	39	191	125210.7	131104.67	3	5893.82	2
801.406	1	40		49	217	817	124780.8	132565.78	2	7784.82	3
804.005	0	50		68	294	792	124377.3	132162.06	4	7784.82	3
810.898	−1	200		239	994	3948	123320.0	131104.67	3	7784.82	3
811.616	−2	70		59	229	642	123210.9	129104.48	3	5893.82	2
814.378	1	30		15	61	247	122793.1	131104.67	3	8311.43	4
814.539	−4	1		3	13	54	122768.8	130552.98	4	7784.82	3
814.616	1	15		15	71	197	122757.3	135027.22	5	12269.73	4
815.987	−1	1		3	19	60	122551.0	147601.42	1	25050.63	0
817.297	0	2		4	957	1099	122354.5	127565.05	4	249919.57	4
818.060 p	7	150		121	490	2002	122240.5	130552.98	4	8311.43	4
819.065	−4	100		195	896	3727	122090.5	134359.66	4	12269.73	4
821.930	1	100		179	651	2560	121664.8	127558.79	2	5893.82	2
827.858	−4	3		5	19	60	120793.6	129104.48	3	8311.43	4
830.152	−1	15		3	646	708	120459.9	131104.67	3	251562.98	2
832.481	−1	40		18	125	359	120122.9	147601.42	1	27478.68	2
834.082	1	1		1	3	20	119892.3	132162.06	4	12269.73	4
834.912 a	6	10		4	13	57	119773.1	127558.79	2	7784.82	3
836.311	−5	10		6	1348	1491	119572.7	127558.79	2	247130.74	1
838.547	−2	100		91	322	1387	119253.9	127565.05	4	8311.43	4
839.543	0	40		19	4058	4569	119112.5	127565.05	4	246677.55	4
840.350 D	2	60		18	98	250	118998.1	139549.81	3	20551.37	2
840.350 D	−6	60		10	2441	2727	118998.1	132565.78	2	251562.98	2
845.426	−2	30		14	55	250	118283.6	130552.98	4	12269.73	4
848.507	−4	3		3	659	727	117854.1	132162.06	4	250015.66	5
849.200	−3	1		3	626	667	117757.9	132162.06	4	249919.57	4
849.444	0	40		23	118	364	117724.1	138275.39	1	20551.37	2

Table 3. Continued.

λ_{exp} (Å)	$\Delta\lambda$ (mÅ)	Int_{exp} PP	IP	Int cal	gA_{CI}	gA_{no-CI}	σ_{exp} (cm^{-1})	E^o (cm^{-1})	J	E^e (cm^{-1})	J
851.653	−4	15		6	1438	1625	117418.7	132597.49	5	250015.66	5
855.995 a	−3	200		737	4358	14190	116823.1	142910.77	5	26088.12	6
860.561	4	20		9	2337	2637	116203.3	135359.21	2	251562.98	2
861.143	−1	3		3	548	588	116124.7	130552.98	4	246677.55	4
864.631	−2	5		4	941	1056	115656.2	134359.66	4	250015.66	5
865.353	1	20		30	6932	7821	115559.8	134359.66	4	249919.57	4
866.776	3	25		33	7530	8445	115370.0	134359.66	4	249730.10	3
867.342	4	30		31	106	501	115294.8	127565.05	4	12269.73	4
867.622	0	25		22	4424	4986	115257.5	131104.67	3	246362.22	2
868.546 p	9	20		.3	54	56	115134.9	127558.79	2	242694.90	3
868.584 p	−1	5		4	663	766	115130.0	127565.05	4	242694.90	3
869.650	−3	50		30	6920	7870	114988.9	135027.22	5	250015.66	5
870.381	1	30		14	3305	3772	114892.2	135027.22	5	249919.57	4
871.020	−1	25		14	64	252	114808.0	135359.21	2	20551.37	2
871.333	1	60		53	235	662	114766.7	135318.28	3	20551.37	2
872.339	1	80	56	46	9033	10180	114634.4	130552.98	4	245187.54	3
872.869	2	15		7	1483	1688	114564.7	132565.78	2	247130.74	1
873.241	−4	5		5	959	1111	114516.0	132162.06	4	246677.55	4
874.034	−1	10		4	975	1109	114412.0	135318.28	3	249730.10	3
874.981	−3	80	49	34	178	590	114288.2	140180.78	2	25892.92	1
876.574	−3	100	36	45	9242	10410	114080.5	132597.49	5	246677.55	4
878.758 p	−4	20	20	18	3746	4210	113797.0	132565.78	2	246362.22	2
879.009	0	10		10	2046	2336	113764.4	133366.26	1	247130.74	1
879.876	0	100	83	106	24470	27580	113652.3	136363.39	6	250015.66	5
880.359	4	5		4	640	709	113590.0	129104.48	3	242694.90	3
883.204	5	40	37	29	142	468	113224.2	138275.39	1	25050.63	0
884.759	3	50	19	25	4841	5498	113025.1	132162.06	4	245187.54	3
884.982	−5	1		1	119	130	112996.7	133366.26	1	246362.22	2
887.294	−1	150		158	818	2689	112702.2	140180.78	2	27478.68	2
887.899 bl	6	120		42	205	664	112625.5	138519.19	0	25892.92	1
888.619	−1	40		16	2805	3129	112534.2	130552.98	4	243086.98	4
889.820	2	80	35	38	185	593	112382.2	138275.39	1	25892.92	1
890.329	−1	15		8	1638	1862	112318.0	134359.66	4	246677.55	4
891.732	5	20		10	1758	1928	112141.3	130552.98	4	242694.90	3
892.292	2	80	37	51	259	754	112070.9	139549.81	3	27478.68	2
892.743D	0	100	109	141	560	2053	112014.4	132565.78	2	20551.37	2
892.743D	−10	100		12	2919	3362	112014.4	139549.81	3	251562.98	2
892.998	0	20			1213	1349	111982.4	131104.67	3	243086.98	4
895.464	−2	50	27	36	5558	6256	111673.9	127558.79	2	239232.46	2
895.662	9	80	30	35	6970	7946	111649.2	135027.22	5	246677.55	4
896.137	1	30	20	21	3608	4074	111590.1	131104.67	3	242694.90	3
897.818	9	15		8	1802	2013	111381.1	140180.78	2	251562.98	2
897.992	−2	5		5	962	1101	111359.5	135318.28	3	246677.55	4
899.852	−1	40		11	1750	1955	111129.4	127558.79	2	238688.04	3
899.905	1	80	67	70	10600	11840	111122.9	127565.05	4	238688.04	3
900.548	3	15		9	1752	1964	111043.5	135318.28	3	246362.22	2
900.876	0	15		7	1369	1560	111003.1	135359.21	2	246362.22	2
901.521a	11	80	29	28	4867	5514	110923.6	132162.06	4	243086.98	4
902.557	3	80	34	34	165	544	110796.3	138275.39	1	27478.68	2
904.708	0	50	23	23	3974	4549	110532.9	132162.06	4	242694.90	3
905.068	4	80	56	53	9376	10550	110489.0	132597.49	5	243086.98	4
906.045	0	30		8	1869	2158	110369.8	139549.81	3	249919.57	4
907.601	−2	80	33	29	6368	7173	110180.6	139549.81	3	249730.10	3
908.034D	9	100		3	557	620	110128.0	132565.78	2	242694.90	3
908.034D	0	100		32	4925	5610	110128.0	129104.48	3	239232.46	2
910.176	3	25		14	2546	2859	109868.9	135318.28	3	245187.54	3
912.542	−3	50	32	33	4965	5612	109583.9	129104.48	3	238688.04	3
912.837	6	20	25	22	4778	5347	109548.6	140180.78	2	249730.10	3
913.522	−1	40	60	69	297	924	109466.5	135359.21	2	25892.92	1
917.947	3	20	16	15	63	197	108938.7	135027.22	5	26088.12	6

Table 3. Continued.

λ_{exp} (Å)	$\Delta\lambda$ (mÅ)	Int_{exp} PP	IP	Int cal	gA_{CI}	gA_{no-CI}	σ_{exp} (cm^{-1})	E^{o} (cm^{-1})	J	E^{e} (cm^{-1})	J
918.653	3	30		10	1929	2148	108855.0	138275.39	1	247130.74	1
919.732	0	5		2	285	355	108727.3	134359.66	4	243086.98	4
920.719	6	20		8	1653	1852	108610.8	138519.19	0	247130.74	1
921.212	4	1		2	6	18	108552.6	129104.48	3	20551.37	2
923.053	−8	3		1	93	93	108336.1	134359.66	4	242694.90	3
923.225	−3	100	30	36	141	436	108316.0	133366.26	1	25050.63	0
924.767	−2	30	20	13	1881	2188	108135.3	130552.98	4	238688.04	3
924.844	13	10		1	190	205	108126.3	131104.67	3	239232.46	2
925.188	6	20		12	2322	2606	108086.1	138275.39	1	246362.22	2
925.415	1	40		16	2810	3183	108059.7	135027.22	5	243086.98	4
926.948	−3	15		6	24	76	107880.9	135359.21	2	27478.68	2
927.304	0	50	36	37	155	488	107839.6	135318.28	3	27478.68	2
927.915	2	20		9	1551	1764	107768.5	135318.28	3	243086.98	4
930.460	−4	40		10	39	121	107473.8	133366.26	1	25892.92	1
931.296	−6	40	18	17	2895	3262	107377.3	135318.28	3	242694.90	3
931.653	−3	50	26	24	4134	4637	107336.1	135359.21	2	242694.90	3
934.508D	5	150		55	11900	13490	107008.2	142910.77	5	249919.57	4
934.508D	−7	150		44	140	512	107008.2	127558.79	2	20551.37	2
936.233	12	3		.4	77	88	106811.0	139549.81	3	246362.22	2
941.772	−12	3		2	457	512	106182.8	140180.78	2	246362.22	2
944.586	−2	40		18	2588	2887	105866.4	133366.26	1	239232.46	2
961.891	−3	40		17	3883	4375	103961.8	147601.42	1	251562.98	2
963.694	−6	30		14	2710	3042	103767.4	142910.77	5	246677.55	4
975.470	−6	10		6	951	1072	102514.7	140180.78	2	242694.90	3
998.232	−9	30		11	1777	2005	100177.1	142910.77	5	243086.98	4
1866.896	9	50		33	3733	4795	53564.9	197997.88	3	251562.98	2
1868.031	−4	30		25	2503	2901	53532.3	193598.54	2	247130.74	1
1895.243	0	8		26	2433	2801	52763.7	193598.54	2	246362.22	2
1899.414	9	100		50	4756	7698	52647.8	194029.49	3	246677.55	4
1902.492	7	150		59	6240	10070	52562.6	197452.83	4	250015.66	5
1905.966	−3	50		18	1880	3020	52466.8	197452.83	4	249919.57	4
1912.874	−3	8		15	1574	2571	52277.4	197452.83	4	249730.10	3
1925.978	0	40		36	3779	4700	51921.7	197997.88	3	249919.57	4
1933.032	0	20		26	2711	3478	51732.2	197997.88	3	249730.10	3
1938.394	−4	30		32	2790	3202	51589.1	193598.54	2	245187.54	3
1954.726	−1	5		18	1551	2557	51158.1	194029.49	3	245187.54	3
2030.842	−4	3		3	294	489	49224.8	197452.83	4	246677.55	4
2190.667D	11	400		26	1862	3015	45633.9	197452.83	4	243086.98	4
2190.667D	0	400		16	1017	1170	45633.9	193598.54	2	239232.46	2
2209.637	−6	100		21	1481	2416	45242.2	197452.83	4	242694.90	3
2211.551	−4	200		17	1082	1770	45203.1	194029.49	3	239232.46	2
2217.127D	6	400		27	1644	1883	45089.4	193598.54	2	238688.04	3
2217.127D	−13	400		23	1629	2098	45089.4	197997.88	3	243086.98	4
2236.596	6	100		16	1164	1499	44696.9	197997.88	3	242694.90	3
2238.515	−3	10		20	1251	2064	44658.6	194029.49	3	238688.04	3

p: line resolved on the plate, but perturbed by a close line.
bl: line partially resolved in a blended emission peak with components of similar intensities.
a: asymmetrical line, when the components of the blend have different intensities.
D: doubly classified.

HFR values for unknown configurations. In this parity, all the configuration interaction (CI) parameters were constrained to keep a constant ratio of their HFR values along the iteration process. By using the initial HFR radial integrals, the levels of the configuration $5p^5 4f^2 6s$ are predicted in the energy range 252000–372000 cm^{-1} and those of $5p^5 4f^2 5d$, in the range 180000–368000 cm^{-1}, so that the four predicted levels of $5p^6 4f6s$ ^3F and ^1F (194000–199000 cm^{-1}) are amid numerous levels of the configuration $5p^5 4f^2 5d$. The adopted parameters of core-excited configurations in Nd V, which take into account corrections of HFR values derived for $5p^5 4f^3$ in Pr IV [8], place the lowest level of $5p^5 4f^2 5d$ near 171000 cm^{-1} and this leads to mixed eigenfunctions for the $5p^6 4f6s$ levels. Indeed, besides a dominant ^3F or ^1F component, about 40% of their eigenfunctions is spread out on many $5p^5 4f^2 5d$ levels. This does not result in large CI energy shifts and the root mean square (rms) deviation for all the 24 levels is as low as 26 cm^{-1} at the final step of the parametric fit. The forbidden $5p^6 4f6p$–$5p^5 4f^2 5d$ transitions that are now enabled by the weak 4f6s components in the eigenfunction of $5p^5 4f^2 5d$ levels

Table 4. Fitted parameters and Hartree–Fock radial integrals (in cm^{-1}) for even-parity configurations of Nd^{4+}. SF is the scaling factor SF = Fitted/HFR.

	$4f^2$				4f6p			
Param.	Fitted	St. dev.	HFR	SF	Fitted	St. dev.	HFR	SF
E_{av}	13629	9			246516	9		
F^2(ff)	84585	125	111118	0.761				
F^4(ff)	59749	334	70158	0.852				
F^6(ff)	38786	216	50600	0.766				
α	17	1						
β	−439	58						
γ	1800	Fixed						
ζ_f	986	5	1063	0.927	1097	5	1158	0.947
ζ_p					4678	14	4006	1.168
F^2(fp)					9688	129	11883	0.815
G^2(fp)					3167	83	2981	1.062
G^4(fp)					2661	147	2780	0.957
C.I. Slater Parameter	Fitted	St. dev.	HFR	SF				
R^2(ff, fp)	−3308	Fixed	−4706	(0.700)				
R^4(ff, fp)	−2053	Fixed	−2920	(0.700)				

Table 5. Fitted parameters and Hartree–Fock radial integrals (in cm^{-1}) for odd-parity configurations of Nd^{4+}. SF is the scaling factor SF = Fitted/HFR.

	4f5d				4f6s			
Param.	Fitted	St. dev.	HFR	SF	Fitted	St. dev	HFR	SF
E_{av}	136400	603			196731	223		
ζ_f	1085	8	1150	0.943	1047	8	1157	0.905
ζ_d	1504	16	1462	1.029				
F^1(fd)	859	147						
F^2(fd)	26354	441	34558	0.763				
F^4(fd)	18936	556	17210	1.100				
G^1(fd)	11743	431	13653	0.860				
G^2(fd)	1869	157						
G^3(fd)	12001	323	12213	0.983				
G^4(fd)	1793	267						
G^5(fd)	8368	291	9638	0.868				
G^3(fs)					4281	324	3813	1.123
C.I. Slater Parameter	Fitted	St. dev.	HFR	SF				
$5p^64f5d–5p^64f6s$								
R^2(fd, fs)	1613	256	2504	0.644				
R^3(fd, sf)	2415	383	3749	(0.644)				
$5p^64f5d–5p^54f^25d$								
R^2(fp, ff)	−10171	−1615	−15789	(0.644)				
R^4(fp, ff)	−5090	−808	−7901	(0.644)				
R^2(pp, fp)	−23501	−3731	−36483	(0.644)				
R^2(pd, fd)	−17668	−2805	−27428	(0.644)				
R^4(pd, fd)	−11394	−1809	−17689	(0.644)				
R^1(pd, df)	−16040	−2547	−24901	(0.644)				
R^3(pd, df)	−11551	−1834	−17932	(0.644)				
$5p^64f5d–5p^54f^26s$								
R^2(pd, fs)	3053	485	4740	(0.644)				
R^1(pd, sf)	1492	237	2316	(0.644)				
$5p^64f6s–5p^54f^25d$								
R^2(ps, fd)	3895	618	6047	(0.644)				
R^3(ps, df)	−1476	−234	−2292	(0.644)				
$5p^64f6s–5p^54f^26s$								
R^2(fp, ff)	−10048	−1595	−15598	(0.644)				
R^4(fp, ff)	−5009	−795	−7776	(0.644)				
R^2(pp, fp)	−23565	−3741	−36583	(0.644)				

have not yet been identified. Small changes in the fixed value of the average energy of $5p^54f^25d$ noticeably modify the compositions of the $5p^64f6s$ eigenfunctions.

In the even parity, the limited CI effects did not allow us to fit the relevant Slater parameters and the scaling factor of 70% applied to their HFR values is an average value derived from previous studies. The radial parameters of $4f^2$ and 4f6p were fitted from the 24 known levels with an rms deviation of 28 cm^{-1}. Tables 4 and 5 report the fitted values of the radial parameters in the even and odd parities, respectively. It is

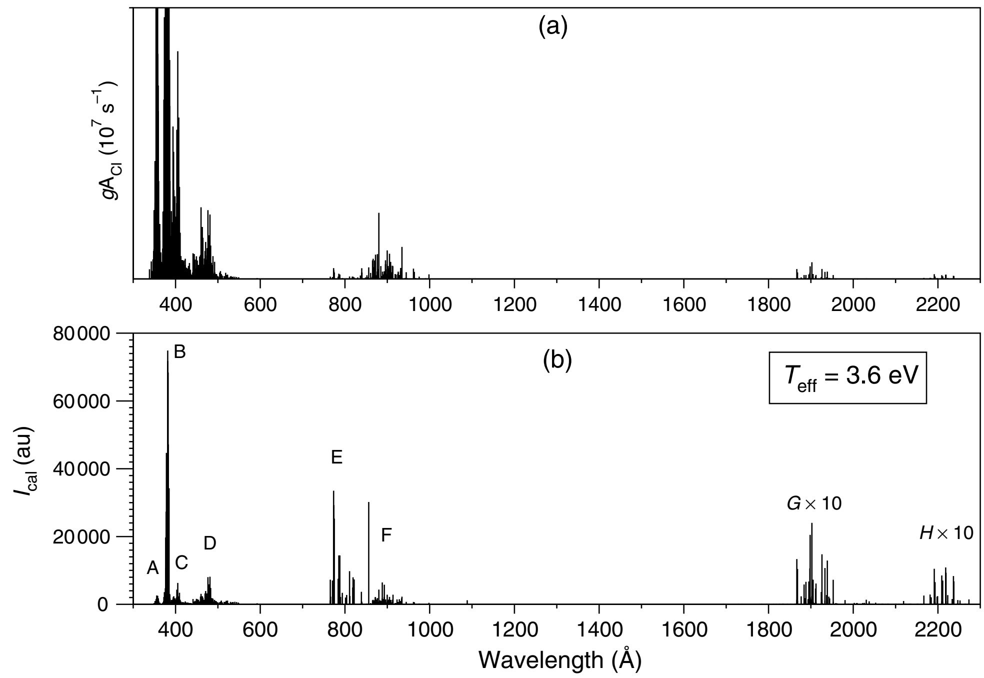

Figure 1. Transitions between the two even- $5p^6(4f^2 + 4f6p)$ and the four odd-parity $5p^6(4f5d + 4f6s)$, $5p^54f^2(5d + 6s)$ configurations of Nd V. In (a) the gA values result from the calculation of 12 configurations. In (b), the intensities I_{cal} (in arbitrary units) include a Boltzmann factor at $T_{eff} = 3.6$ eV. The peaks A and C denote 5p–6s transitions, the peaks B and D 5p–5d transitions, the arrays E and F the 4f–5d and 5d–6p transitions. For the arrays G and H (the 6s–6p transitions), the intensities are multiplied by a factor of 10. A detailed view of (b) around 900 Å is shown in figure 2(c).

seen that the effective parameters representing the interaction of 4f5d with far configurations (f^1(4f, 5d), G^2(4f, 5d) and G^4(4f, 5d)) have well-defined values, i.e. small standard deviations, and they are consistent with values derived from the levels of $4f^25d$ in Nd IV [2].

5. Transition probabilities

The final radial parameters in the approximation including 8 even-parity and 4 odd-parity configurations are used to obtain the values of transition probabilities gA_{CI}, represented in the figure 1(a), where g is the statistical weight of the upper level and A_{CI} is the Einstein coefficient. For the sake of simplicity, and further comparisons with experimental spectra, only the strongest transitions starting from 4f6p, or ending on $4f^2$ are drawn. The prominent transitions are $5p^64f^2$–$5p^54f^26s$ (emission peaks labelled A and C on figure 1(b)) and $5p^64f^2$–$5p^54f^25d$ (peaks B and D). The transitions $4f^2$–4f5d and 4f5d–4f6p overlap (peaks E and F) between 720 and 1000 Å. The 4f6s–4f6p transitions split into sub-arrays according to jj coupling selection rules (arrays G and H).

In table 3, the probabilities gA_{CI} defined in the previous paragraph are compared with gA_{no-CI} values derived from one-configuration parametric study of the four known configurations $4f^2$, 4f6p, 4f5d and 4f6s. Depending on the configurations involved in the transitions, systematic differences can be noticed between the two approximations. The 4f6p–4f5d transitions are about 10% weaker in the CI than in the no-CI approach. The 4f6p–4f6s transition probabilities are proportional to the squared amplitudes of the 4f6s components in the eigenfunction of the high odd levels and are therefore reduced in the CI option.

Of all the calculated transition probabilities, those of the 4f5d–$4f^2$ transitions show the largest changes when CI effects are taken into account, since they are then reduced by a factor of 3 to 4, although the admixtures of $5p^54f^25d$ components in the $5p^64f5d$ eigenfunctions do not exceed 2.67% (see table 2). This is characteristic of the quenching of a transition array by another array [15, 16]. Indeed, the $5p^64f^2$–$5p^54f^25d$ transition array is predicted to have strong lines located in a narrow *emissive zone* [17] around 380 Å. They have probabilities larger than those of $5p^64f^2$–$5p^64f5d$ transitions by more than two orders of magnitude. This is a consequence of the core excitation $5p^6(^1S_0)4f^2$–$5p^55d(^1P)4f^2$ with a large Slater exchange integral G^1(5p, 5d) and the $4f^2$ group acting as spectator electrons. As an example, the 5p–5d transition of $5p^6(^1S)4f^2\ ^3H_6$–$5p^55d(^1P)4f^2\ ^3H^o_6$ has $gA_{CI} = 1.595(10^{12})\ s^{-1}$ slightly larger than $gA_{no-CI} = 1.556(10^{12})\ s^{-1}$, whereas the 4f–5d transition of $5p^64f^2\ ^3H_6$–$5p^64f5d\ ^3H^o_6$ has $gA_{CI} = 0.935(10^9)\ s^{-1}$ much weaker than $gA_{no-CI} = 3.913(10^9)\ s^{-1}$.

Systematic comparisons of measured and calculated transition probabilities through lifetimes of levels are possible [18]. They have been done for a number of lanthanide II and III spectra, but not for the V spectra because of the absence of experimental data.

6. Determination of an effective excitation temperature in the spark from line intensities

Some of the recently recorded spectra used IPs which have a linear intensity response over a much wider dynamic range than that of the PPs. One exposure on an IP (tritium-sensitive

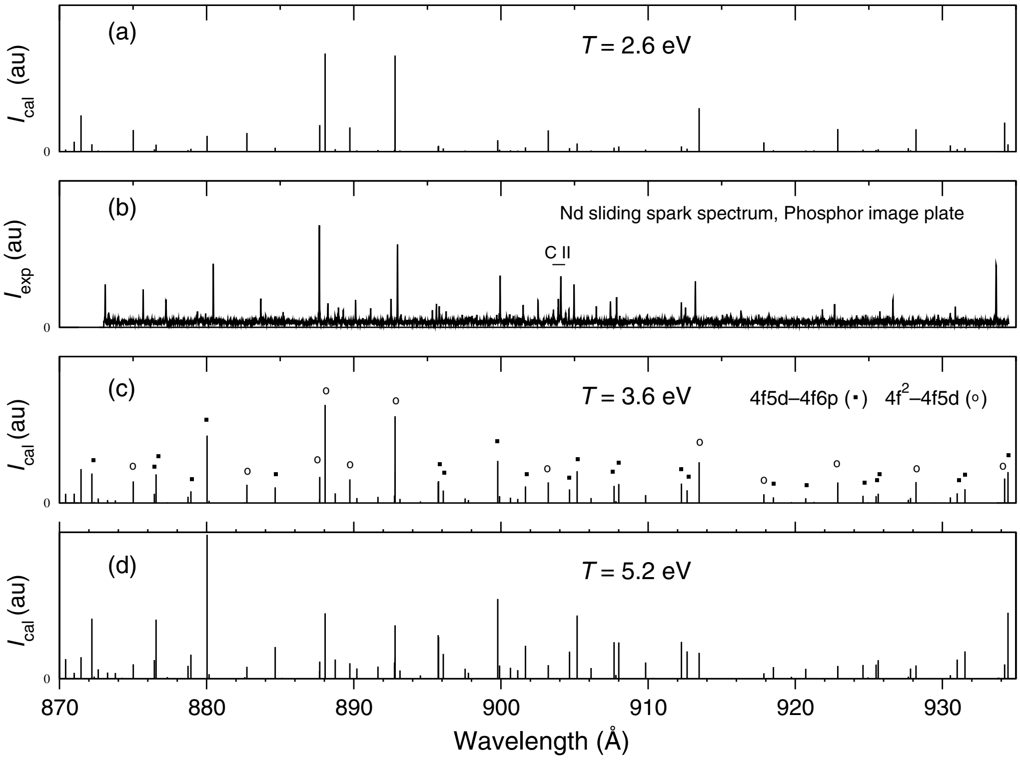

Figure 2. Comparison of a spark spectrum of Nd sliding spark recorded on a phosphor IP (b) with calculated wavelengths and intensities for $T = 2, 6$ eV (a), 3.6 eV (c) and 5.2 eV (d). Two types of transitions 4f–5d and 5d–6p are labelled with circles and dots, respectively. The used gA_{CI} transition probabilities result from the calculation of 12 configurations, five of them with open-core $5p^5$.

storage phosphor screen from Perkin-Elmer[5]) integrating over about 3000 sparks covered the range 872–935 Å and was scanned with a Fuji FLA7000 [19] scanner. The experimental spectrum is represented in figure 2(b). Nearly all the lines belong to Nd V, except for four impurity lines of ionized carbon near 904 Å. In this section, we will take advantage of the properties of IPs to show the effect of CI on line intensities.

The classified lines around 900 Å show that, for calculated transition probabilities of similar magnitudes, observed intensities are much smaller for the 4f6p–4f5d than for the 4f5d–$4f^2$ transitions likely due to different populations of the upper levels. Thermal equilibrium cannot be assumed in the sliding spark. However, by assuming that these populations follow the Boltzmann law, it is possible to define an excitation temperature. The calculated line intensities I_{cal} are then proportional to $(gA/\lambda)\exp(-E_{\mathrm{u}}/kT)$, where E_{u} is the energy of the upper level, and T is the excitation temperature. They have been calculated for three temperatures of 2.6, 3.6 and 5.2 eV using the gA_{CI} values of table 3 and show noticeable differences in figure 2 where they are also compared to the experimental spectrum.

Since we have two transition arrays from two configurations which show a difference of average energies much larger (13.6 eV) than the quantity kT, we could take advantage of their intensity ratio for deriving a reliable estimate of the effective excitation temperature of the spark source. Indeed, the experimental intensity I_{exp} of a line is linearly related to the calculated one I_{cal} by some unknown efficiency factor F which depends on the experimental setup and is independent of the temperature, i.e. $I_{\mathrm{exp}}/I_{\mathrm{cal}}(T) = F$. Therefore, we selected 11 lines of the $4f^2$–4f5d transitions and 18 lines of the 4f6p–4f5d transitions that appeared on the same exposure in a limited wavelength interval of 65 Å within which the variation of the efficiency factor versus wavelength can be neglected. By equating the averages of the ratio $I_{\mathrm{exp}}/I_{\mathrm{cal}}(T)$ from the two sets of lines, we may determine the effective temperature T_{eff} as a solution of the equality. In practice, we performed a graphic resolution by plotting the two averages as functions of temperature and taking the abscissa of the crossing point as shown in figures 3(a) and (b). In order to reduce the vertical scale of the graphs, the experimental intensities I_{exp} of both the transition arrays were multiplied by the same scaling function $\exp[-(E_{\mathrm{av}}^{\mathrm{fd}} + E_{\mathrm{av}}^{\mathrm{fp}})/2kT]$, where $E_{\mathrm{av}}^{\mathrm{fd}}$ and $E_{\mathrm{av}}^{\mathrm{fp}}$ are the average energies of the levels of the corresponding transition arrays. The uncertainties of the $I_{\mathrm{exp}}/I_{\mathrm{cal}}$ ratios depend on several weak I_{exp} values taken with a low signal-to-noise ratio and a conservative uncertainty of 0.3 eV seems appropriate for T_{eff}.

It is worth pointing out that plasma diagnostics depend on the quality of the atomic data used in the model. In order to show the importance of taking into account CIs in theoretical calculations, we performed two determinations of T_{eff} using I_{cal} derived from gA_{CI} then from $gA_{\mathrm{no\text{–}CI}}$, corresponding to the graphs of figures 3(a) and (b), respectively. On figure 3(a), the curves cross at $T_{\mathrm{eff}} = 3.6$ eV. On figure 3(b), where the CIs are not taken into account, we obtained a very different temperature $T_{\mathrm{eff}} = 5.2 \pm 0.4$ eV. Obviously, the larger basis set gives a better representation of the atomic system, therefore, we used the gA_{CI} values and $T_{\mathrm{eff}} = 3.6$ eV for deriving the I_{cal} values collected in table 3. As a confirmation,

[5] Commercial products are identified for adequate specification of the experimental procedure. This identification does not imply recommendation or endorsement by NIST.

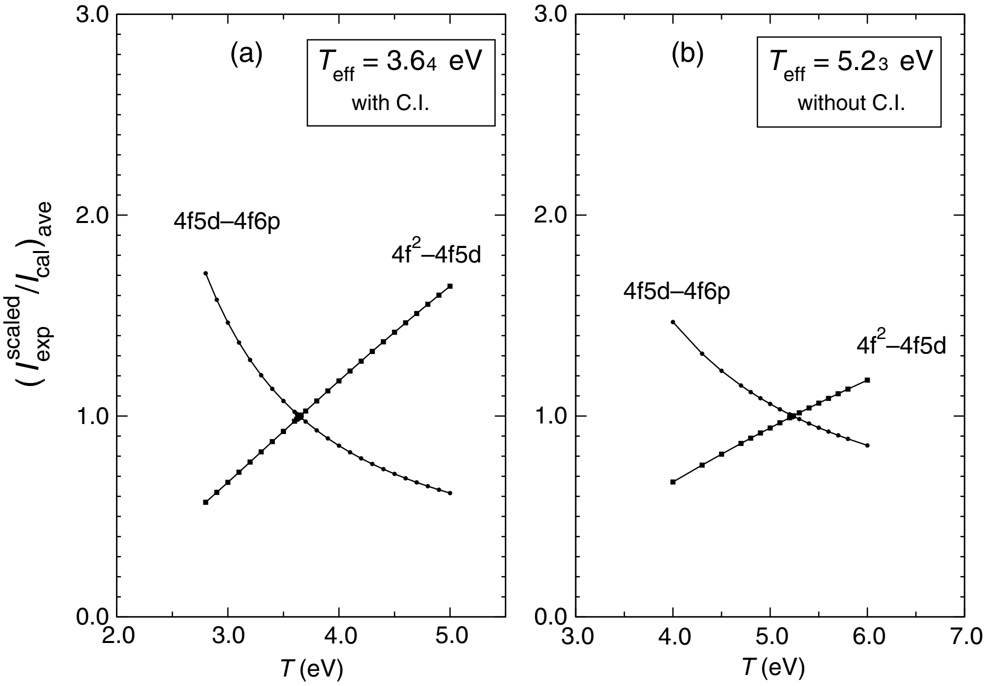

Figure 3. Determination of an effective temperature of population in the sliding spark by comparing the intensity scalings of the transitions 4f–5d and 5d–6p at various effective temperatures. The case (a) uses a 12 configurations basis with $5p^5$ core-excited configurations, the case (b) neglects the CI effects. The same scaling function was applied to experimental intensities of both transition arrays (see text).

one can see in figure 2, especially from the pattern formed by the lines at 880, 888, 893 and 900 Å, as well as the three lines around 913 Å, that a good agreement between experimental and calculated intensities is obtained for an excitation temperature of $T_{eff} = 3.6$ eV.

7. Conclusion

The first analysis of a complex fifth spectrum of a lanthanide is achieved in the case of Nd V. Forty-eight levels classify 160 lines and are interpreted by means of the parametric method used by the Cowan codes, starting from HFR evaluations of radial integrals. It is shown that the unknown core-excited configurations $5p^54f^3$ and $5p^54f^25d$, respectively, are the main perturbers of $5p^64f^2$ and $5p^64f5d$, with important consequences for transition probabilities of the 4f–5d resonance lines. In particular, when the $5p^64f5d$–$5p^54f^25d$ interaction is taken into account, the estimated effective excitation temperature in the spark T_{eff} is reduced from 5.2 to 3.6 eV. This should be considered as a warning for plasma diagnostics in weakly charged lanthanide ions. This determination of T_{eff} is a tool of high interest for supplying realistic predictions of the observed intensities in unclassified spectra. Finally, the well-isolated levels of $5p^64f^2$ are of interest for far-CI effects studies following [19], now described in [20].

Acknowledgments

AM is grateful to the Société de Secours des Amis des Sciences for the financial support of his research in 2005 and 2007. The financial support of the French CNRS-PNPS program is acknowledged. WULTB and NC wish to thank the RAYTEST company for letting them use a Fuji scanner for image plates. Laboratoire Aimé Cotton is in association with Université Paris-Sud 11. We are indebted to Drs J Reader and A Kramida at NIST for their valuable suggestions in the preparation of the manuscript.

References

[1] Wyart J-F *et al* 2006 *J. Phys. B: At. Mol. Opt. Phys.* **39** L77
[2] Wyart J-F *et al* 2006 *J. Phys. B: At. Mol. Opt. Phys.* **40** 3957
[3] Martin W C, Zalubas R and Hagan L 1978 *Atomic Energy Levels, The Rare-Earth Elements* NSRDS-NBS 60
[4] Bockasten K 1955 *Ark. Fysik* **9** 457
[5] Sugar J 1963 *J. Opt. Soc. Am.* **53** 831
[6] Reader J, Sansonetti C J and Deslattes R D 2000 *Appl. Opt.* **39** 627
[7] Kelly R L 1987 *J. Phys. Chem. Ref. Data* **16** 1
[8] Cowan R D 1981 *The Theory of Atomic Structure and Spectra* (Berkeley, CA: University of California Press)
[9] Wyart J-F, Blaise J and Worden E F 2005 *J. Sol. State Chem.* **178** 589
[10] Wyart J-F *et al* 2001 *Phys. Scr.* **63** 113
[11] Redfors A and Reader J 1991 *Phys. Rev.* A **43** 2367
[12] Radziemski L J Jr, Fischer K J and Steinhaus D W 1970 Los Alamos National Laboratory Report No. LA-4402
Radziemski L J Jr and Kaufman V 1969 *J. Opt. Soc. Am.* **59** 424
[13] Mohr P J, Taylor B N and Newell D B 2007 *The 2006 CODATA Recommended Values of the Fundamental Physical Constants (Web Version 5.0)*. Available Online at http://physics.nist.gov/constants
[14] Racah G 1950 *Physica* **16** 651
[15] Bauche J *et al* 1987 *J. Phys. B: At. Mol. Phys.* **20** 1443
[16] Bauche J and Bauche-Arnoult C 1996 *Phys. Scr.* T **65** 99
[17] Bauche J *et al* 1983 *Phys. Rev.* A **28** 829
[18] Biémont E 2005 *Phys. Scr.* T **119** 55
[19] Judd B R 1985 *Rep. Prog. Phys.* **48** 907
[20] Wyart J-F *et al* 2008 *J. Phys. B: At. Mol. Opt. Phys.* **41** 085001